IEEE Photonics Journal
An IEEE Photonics Society Publication

Silicon On-Chip One-Dimensional Photonic Crystal Nanobeam Bandgap Filter Integrated With Nanobeam Cavity for Accurate Refractive Index Sensing

Volume 8, Number 2, April 2016

Daquan Yang
Chuan Wang
Yuefeng Ji

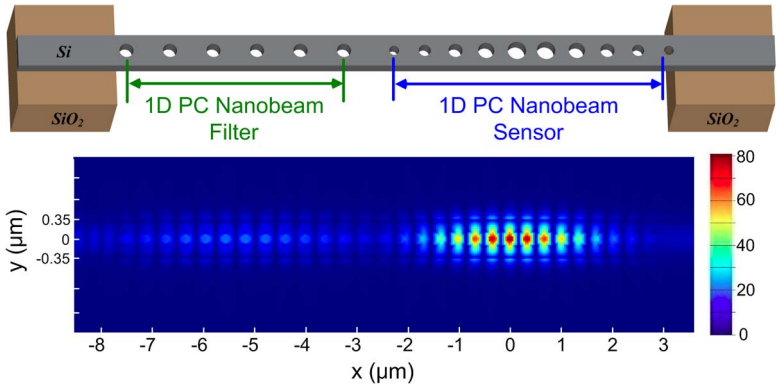

DOI: 10.1109/JPHOT.2016.2536942
1943-0655 © 2016 IEEE

Silicon On-Chip One-Dimensional Photonic Crystal Nanobeam Bandgap Filter Integrated With Nanobeam Cavity for Accurate Refractive Index Sensing

Daquan Yang,[1,2] Chuan Wang,[1] and Yuefeng Ji[1,2]

[1]State Key Laboratory of Information Photonics and Optical Communications, Beijing University of Posts and Telecommunications, Beijing 100876, China
[2]School of Information and Communication Engineering, Beijing University of Posts and Telecommunications, Beijing 100876, China

DOI: 10.1109/JPHOT.2016.2536942

Manuscript received January 20, 2016; revised February 20, 2016; accepted February 25, 2016. Date of publication March 1, 2016; date of current version March 11, 2016. This work was supported in part by the Natural Science Foundation of China under Grant 61501053 and Grant 61471050, by the National 973 Program under Grant 2012CB315705, and by the Fund of the State Key Laboratory of Information Photonics and Optical Communications (BUPT: IPOC2015ZC03) and the Fundamental Research Funds for the Central Universities (BUPT), China. Corresponding author: D. Yang (e-mail: yangdq5896@163.com).

Abstract: A novel method for integration of high-performance 1-D photonic crystal nanobeam bandgap filter (1-D PC-NBF) and high-sensitivity 1-D PC nanobeam cavity sensor (1-D PC-NCS) is proposed on a monolithic silicon chip. The 1-D PC-NBF consists of a simple 1-D PC nanobeam waveguide, in which the bulk air-hole grating radii are kept the same. The 1-D PC-NCS consists of a common 1-D PC nanobeam cavity, in which the air-hole grating radius is parabolically tapered from center to end. By using the 3-D finite-difference time-domain (3-D-FDTD) method, the proposed 1-D PC-NBF with an effective low-pass bandgap ranging from 1533 to 1785 nm (with width > 250 nm) is demonstrated, where the resonant wavelengths lying in the bandgap are not guided. Then, by connecting an additional 1-D PC-NBF to a 1-D PC-NCS in series, a transmission spectrum only containing the specific fundamental mode of the 1-D PC nanobeam cavity for sensing purposes is created, while the other high-order modes are filtered out. Moreover, the additional 1-D PC-NBF has no influence on the properties (e.g., *Q*-factor, resonance position, and sensitivity) of the fundamental resonant mode of 1-D PC-NCS. In particular, the footprint of the proposed 1-D PC nanobeam integrated sensor is ultracompact around 0.7 μm $\times$ 10 μm, which is improved more than three orders of magnitude compared with the integrated sensor devices based on 2-D PC. Thus, the method presented here is promising to build highly parallel integrated sensor arrays for lab-on-a-chip applications and accurate detections.

Index Terms: Integrated nanophotonic, optical interconnect, photonic crystals, sensors, bandgap filters, 3-D-finite-difference time-domain (3-D-FDTD).

1. Introduction

In the past decade, ultra-high *Q*-factor (Q) and ultra-low mode volume (V_m) 1-D photonic crystal (PC) nanobeam cavities [1]–[7] have been demonstrated as a promising candidate for different applications, e.g., nanobeam lasers [8], drop filters [9], electro-optical modulators [10],

nanoparticle trapping [11], optomechanical device[12], quantum dots [13], nano light emitting diodes (LEDs) [14], [15], and slow-light enhanced nonlinear phenomenon [16]. In particular, due to the ultra-high Q/V_m optical resonator enabling the enhancement of light-matter interactions, 1-D PC nanobeam cavities have recently attracted considerable interest for lab-on-a-chip optical sensing [17] with high figures of merit (FOMs) [18]–[25]. For example, as shown in our previous works [21], [24], a real-time and label-free biosensor based on nanoslotted parallel multi-nanobeam integrated 1-D PC cavity have theoretically and experimentally demonstrated with unexplored high sensitivity and high Q-factor, featuring a sensor FOM > 2000, an order of magnitude improvement over previous optical sensors based on traditional 2-D PC cavities. (Here, the sensor FOM $= S \cdot Q/\lambda_{\text{res}}$, where $S = \Delta\lambda/\Delta n$ characterizes the shift of resonance $(\Delta\lambda)$ in response to the surrounding index change (Δn), λ_{res} is the cavity resonance wavelength, and Q is the quality factor [26].) Moreover, the biosensors based on 1-D PC nanobeam cavities have been experimentally reported that ultra-low detection limit ~10 zM of streptavidin in the phosphate buffered saline solution (PBS) [24] and single polystyrene nanoparticle detection with radii down to 12.5 nm [22], [23] can be achieved.

However, the longer strip-shaped 1-D PC nanobeam cavities have several resonant wavelengths in the transmission spectrum [27], which makes them difficult to be used for multiplexed sensing, because the sensing signal of every 1-D PC nanobeam cavity may interact each other due to the crosstalk among multi-cavity parallel sensing. Moreover, it also makes them difficult for future smart screening detection because it easily results in choosing a wrong resonant wavelength (e.g., other high-order low-Q modes) for multiplexed sensing detection rather than the fundamental mode (FM) during the practical detection process. This will lead to the sensing detection being difficult and inaccurate.

Herein, to overcome the limitations mentioned above, a novel method for silicon on-chip integration of 1-D PC nanobeam bandgap filter (1-D PC-NBF) and 1-D PC nanobeam cavity sensor (1-D PC-NCS) is demonstrated. The proposed sensor device is formed by series-connected 1-D PC-BNF and 1-D PC-NCS to filter out other high-order modes in the transmission spectrum. And only the specific fundamental mode (FM) retained for sensing purpose. By using 3-D finite-difference time-domain (3-D-FDTD) method (Lumerical Solutions Inc. Canada), an effective low-pass bandgap ranging from 1533 nm ~ 1785 nm (with width > 250 nm) of 1-D PC-NBF is presented. The refractive index sensitivity of 1-D PC-NCS as high as 123.3 nm/RIU is observed. Particularly, the footprint of the proposed 1-D PC nanobeam integrated sensor is ultra-compact around 0.7 μm $\times$ 10 μm, which is more than three orders of magnitude decreased compared to 2-D PC integrated sensor devices [28], [29]. Thus, the method presented in this work is promising for building ultra-compact lab-on-chip sensors array with high density and parallel-multiplexing capability.

The organization of this paper is as follows. In Section 2, we first describe 1-D PC-NBF design in detail. In Section 3, we describe 1-D PC-NCS design in brief. In Section 4, a method for silicon on-chip integration of 1-D PC-NBF and 1-D PC-NCS in series is demonstrated. Finally, in Section 5, we draw a brief conclusion.

2. 1-D Photonic Crystal Nanobeam Bandgap Filter (1-D PC-NBF) Design

Recently, even though several different kinds of on-chip photonic band-pass filters based on different structures, including 2-D PC waveguides (PCWs) [29], arrayed waveguide gratings (AWGs) [30], micro ring resonators (MRRs) [31], and waveguide Bragg gratings (WBGs) [32], have been previously demonstrated. However, the footprints of those filters above are usually too large. For example, the footprints of the photonic band-pass filter demonstrated in [29] and [30] are as large as $\sim$ 50 μm $\times$ 275 μm and $\sim$ 200 μm $\times$ 350 μm, respectively, which are not suitable for dense integration. In addition, the size of those filters does not match with 1-D PC nanobeam devices. Thus, in this work, a photonic bandgap filter based on 1-D PC nanobeam waveguide is displayed. It is a natural good choice since the sensor element is also made from 1-D PC nanobeam cavity, which makes the transmission alignment easier. Fig. 1 display the

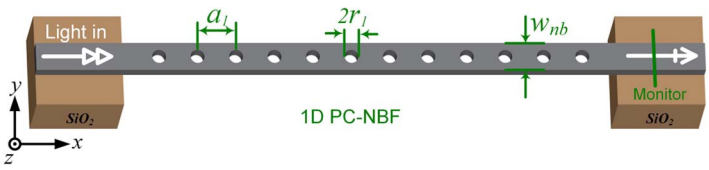

Fig. 1. Schematics of the single silicon 1-D PC nanobeam bandgap filter (1-D PC-NBF). The radius of air-hole gratings are kept in same as $r_1 = 90$ nm. The structure is symmetric with respect to its center. Periodicity $a_1 = 390$ nm is the center-to-center distance between the gratings; $w_{nb} = 700$ nm is the width of the 1-D PC nanobeam waveguide. The thickness of the silicon ridge waveguide is 220 nm. $n_{si} = 3.46$, and $n_{air} = 1.0$.

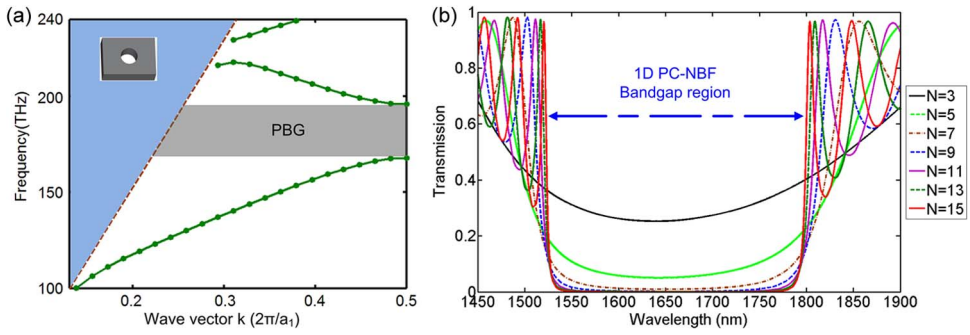

Fig. 2. (a) TE band diagram of the single 1-D PC nanobeam waveguide with $r_1 = 90$ nm, $w_{nb} = 700$ nm, and $a_1 = 390$ nm. The thickness of the nanobeam waveguide is 220 nm. (Inset) Unit cell of waveguide used in the band structure calculation. (b) Transmission spectra obtained by using 3-D-FDTD calculation for different grating number (N), while other structure parameters keep fixed.

schematic of the single 1-D PC-NBF described in this paper. It consists of a simple 1-D PC nanobeam waveguide, which is formed by a series (N) of air-hole gratings $(n_{air} = 1.0)$ punched into a silicon $(n_{si} = 3.46)$ ridge waveguide. The waveguide width is 700 nm $(w_{nb} = 700$ nm$)$. The bulk air-hole gratings radius are kept in the same as $r_1 = 90$ nm. The thickness of the silicon ridge waveguide is 220 nm and the periodicity of the gratings is $a_1 = 390$ nm. The structure is symmetric with respect to the center.

Fig. 2(a) shows the TE band diagram of 1-D PC-NBF with air-hole radii $r_1 = 90$ nm, obtained from 3-D-FDTD simulation with Bloch boundary conditions. The inset is the unit cell of waveguide used in the band structure calculation. Numerical simulations have demonstrated that as the effective refractive index increased (e.g., by reducing air-hole grating radius), the photonics bandgap (PBG) of the structure moves to lower frequency [33]. Thus, with proper engineering of the structure parameters of 1-D PC-NBF, an arbitrary wavelength range bandgap can be obtained. As seen in Fig. 2(a), the photonic bandgap (PBG) ranging from 168.07 THz~195.69 THz is obtained.

Next, in order to achieve a wide low-pass band with sharp shutoff frequency in transmission spectrum, it is necessary to discuss the number (N) of air-hole gratings in 1-D PC-NBF. Fig. 2(b) shows the low-pass bandgap region in the 1-D PC-NBF transmission spectrum as a function of the number (N) of gratings changed. As seen, as the number (N) of gratings increased from $N = 3$ to $N = 15$, both edges of shutoff frequency of the proposed 1-D PC-NBF turn sharper. When the number of gratings $N = 15$, a wide low-pass bandgap with width > 250 nm, ranging from 1533 nm ~ 1785 nm, in the transmission spectrum is observed, which agrees well with PBG obtained from band diagram calculation [see Fig. 2(a)]. The resonant wavelengths lying in the bandgap region of 1-D PC-NBF cannot be guided. On the contrary, the resonances outside the bandgap region are allowed to pass and be used for sensing. In addition, it is worth mentioning that even though the number of gratings N is as large as 15, the footprint of the proposed 1-D

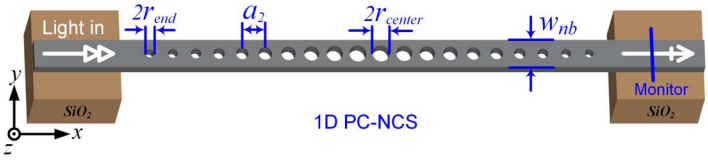

Fig. 3. Schematics of the single silicon 1-D PC nanobeam cavity sensor (1-D PC-NCS). The structure is also symmetric with respect to its center. The number of Gaussian mirror segments is i_{max}, without additional mirrors outside of the Gaussian mirror region. Here, periodicity $a_2 = 330$ nm, $w_{nb} = 700$ nm, the air-hole radius is parabolically tapered from $r_{center} = 120$ nm in the center to $r_{end} = 85$ nm on both sides, i.e., $r(i) = r_{center} + (i-1)^2(r_{end} - r_{center})/(i_{max} - 1)^2$ (i increases from 1 to i_{max}), the thickness of the silicon ridge waveguide is 220 nm, $n_{si} = 3.46$, and $n_{air} = 1.0$.

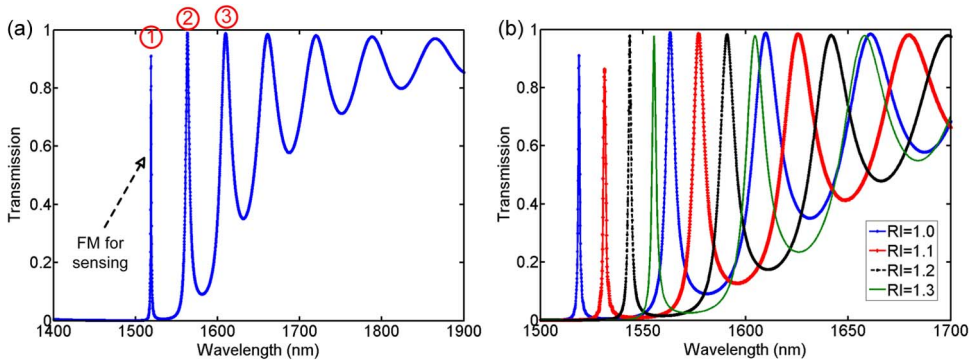

Fig. 4. (a) 3-D-FDTD transmission spectrum of the proposed 1-D PC-NCS device. (b) Composed transmission spectra of the proposed 1-D PC-NCS as a function of RI changed from RI = 1.0 to RI = 1.3.

PC-NBF is only $\sim 0.7\ \mu\text{m} \times 6\ \mu\text{m}$, more than four orders of magnitude decreased compared with the photonic bandpass filter based on AWGs [30]. Thus, the described 1-D PC-NBF here is a good choice to be used as an additional filter to select a specific resonant mode for sensing purpose by connecting a 1-D PC nanobeam cavity sensor in series.

3. 1-D Photonic Crystal Nanobeam Cavity Sensor (1-D PC-NCS) Design

The schematic of the single 1-D PC-NCS described in this paper is shown in Fig. 3. It consists of a 1-D PC nanobeam cavity. The cavity design follows recently discovered deterministic high-Q ($> 10^7$) and high-sensitivity (> 800 nm/RIU, RIU = refractive index unit) recipe [5], [20]–[27]. As seen, the proposed 1-D PC-NCS consists of air-holes $(n_{air} = 1.0)$ in decreasing radii, etched into a silicon $(n_{si} = 3.46)$ ridge waveguide with a width of 700 nm $(w_{nb} = 700\ \text{nm})$. The thickness of the waveguide is $h = 220$ nm and the periodicity of the air holes is $a_2 = 330$ nm. The structure is symmetric with respect to its center. The radius of the center grating of the cavity is $r_{center} = 120$ nm. To create a Gaussian mirror [27], the radius is parabolically tapered from $r_{center} = 120$ nm in the center to $r_{end} = 85$ nm on both sides, i.e., $r(i) = r_{center} + (i-1)^2(r_{end} - r_{center})/(i_{max} - 1)^2$ (i increases from 1 to i_{max}; and i_{max} is the grating number in the Gaussian mirror taper region of 1-D PC-NCS [21].), while the nanobeam waveguide width (w_{nb}) and thickness are kept fixed.

By using the 3-D-FDTD method, Fig. 4(a) shows the transmission spectrum of 1-D PC-NCS displayed in this work. As seen, except for the fundamental mode (FM, i.e., ①) at short wavelength used for sensing, there are also several high-order modes (②, ③). Fig. 4(b) displays the composed transmission spectra as a function of increased refractive index (RI) changed from RI = 1.0 to RI = 1.3. As seen, all three mentioned resonant wavelengths shift (red-shift) as the

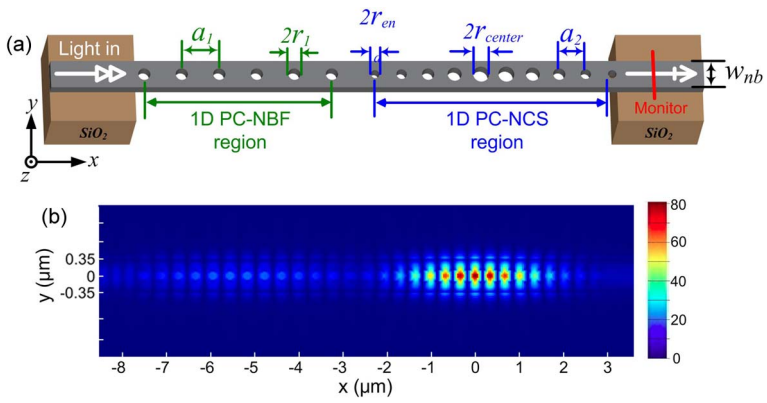

Fig. 5. (a) Schematic of proposed silicon 1-D PC nanobeam bandgap filter for 1-D PC sensor, formed by series-connected 1-D PC-NBF and 1-D PC-NCS. (b) 3-D-FDTD simulation of the major field distribution profile (|Ey|) of the fundamental resonant mode (at 1519.26 nm) in the proposed 1-D PC nanobeam sensor based on 1-D PC nanobeam bandgap filter series-connected 1-D PC nanobeam cavity sensor. Here, periodicity $a_1 = 390$ nm, $a_2 = 330$ nm, $w_{nb} = 700$ nm, $n_{si} = 3.46$, $n_{air} = 1.0$, and the thickness of the silicon 1-D PC nanobeam waveguide is 220 nm. The unit of the x/y axis is micrometers.

function of the refractive index increased. The calculated RI sensitivity of the FM is as high as 122.8 nm/RIU. However, when the RI increases to RI = 1.3 (green line), we find that the FM used for sensing is pressed close to the second high-order mode (②) with RI = 1.0 (blue dot line). For example, if multiple cavity sensors are integrated simultaneously, the output transmission from multiple cavity sensors will be combined at the output, resulting in the issue of mixing of higher order resonance with fundamental mode. That makes them difficult to be used for multiplexed sensing because the sensing signal of every cavity may interact with each other (i.e., crosstalk in multi-cavity parallel sensing). In addition, it also makes them difficult to achieve smart screening detection because it easily results in choosing a wrong resonant mode (e.g., other high-order low-Q modes) for multiplexed sensing detection rather than the preset fundamental mode (FM) during the practical detection process.

4. A Method for the Integration of 1-D PC-NBF Series-Connected 1-D PC-NCS

In this section, to solve the problems mentioned above in Section 3, a novel method for the integration of 1-D PC-NBF and 1-D PC-NCS to filter out the other high-order modes [see ②, ③ in Fig. 4(a)] and only retain the fundamental mode (FM, ①) is demonstrated on a monolithic silicon platform. The schematic is displayed in Fig. 5(a). As seen, the proposal integrated 1-D PC nanobeam sensor device is composed by connecting an additional 1-D PC-NBF to a 1-D PC-NCS in series, which consists of two parts. i) The first part element is 1-D PC-NBF, which consists of single 1-D PC nanobeam waveguide with a wide low-pass bandgap ranging from 1533 nm ~ 1785 nm. The periodicity $a_1 = 390$ nm, and the radius of air-hole gratings are kept the same as $r_1 = 90$ nm. ii) The second part element is 1-D PC-NCS, which consists of single 1-D PC nanobeam cavity with an ultra-high Q factor > 10^7 of the resonance peak of fundamental mode at $\lambda_{res} = 1519.26$ nm. The periodicity $a_2 = 330$ nm. The radius of air-hole gratings are quadratically tapered from $r_{center} = 120$ nm to $r_{end} = 85$ nm, which is the same as displayed in Section 3. The thickness and width of the silicon ridge waveguide are $h = 220$ nm and $w_{nb} = 700$ nm, respectively. In addition, the gap size between 1-D PC-NBF and 1-D PC-NCS in Fig. 5(a) is arbitrary and unfixed, which has no effect on the transmission spectrum of the integrated 1-D PC nanobeam sensor device. With the 3-D-FDTD method, Fig. 5(b) shows the top view of the major field distribution profile (|Ey|) of the fundamental mode (at $\lambda_{res} = 1519.26$ nm) in the integrated sensor device mentioned above. It can be seen clearly that the majority of

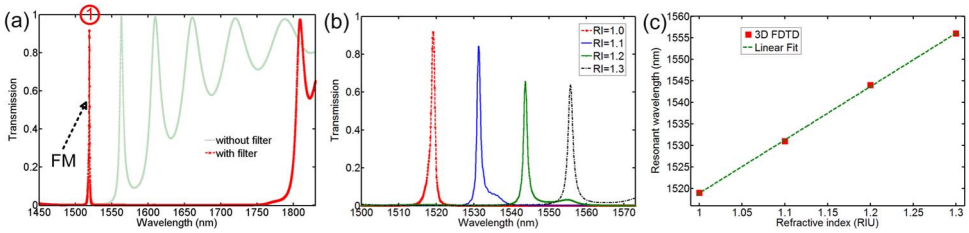

Fig. 6. (a) 3-D FDTD transmission spectra. The red dashed-dot line represents the transmission of proposed 1-D PC-NBF integrated with 1-D PC-NCS by connecting an additional 1-D PC nanobeam bandgap filter to a 1-D PC nanobeam cavity in series. The light green solid-dot line, which is displayed for comparison, represents the transmission of 1-D PC-NCS without series-connected 1-D PC-NBF. (b) Composed transmission spectra of the proposed 1-D PC sensor when the RI changes from RI = 1.0 to RI = 1.3. (c) Resonant wavelength shift (red-shift) as the function of the RI increases.

electric field is strongly localized in the center of 1-D PC-NCS cavity, indicating that a strong interaction between the analytes and the cavity mode can be achieved. Thus, the proposed 1-D PC nanobeam integrated sensor device in this paper is potentially an ideal platform for dense sensors-array design and refractive-index based multiplexed sensing.

Next, in order to save the simulation time for the time domain transmission calculation, we use a high transmission but low Q-factor geometry: for 1-D PC-NBF the number of air-hole gratings is chosen to be $N = 12$; and for 1-D PC-NCS the number of air-hole gratings is chosen to be $i_{max} = 9$, and no additional mirror segments are placed outside of the Gaussian mirror region [18]. With 3D-FDTD simulation, the total transmission spectrum of the proposed 1-D PC-NBF integrated with 1-D PC-NCS is shown as the red dashed-dot line in Fig. 6(a), while the light green solid-dot line which is displayed for comparison represents the transmission of 1-D PC-NCS without series-connected 1-D PC-NBF. See from Fig. 6(a), as expected, by connecting an additional 1-D PC-NBF in series, a transmission of 1-D PC nanobeam cavity sensor only containing the specific fundamental mode (FM) for sensing purpose is created, while the other high-order resonances lying in the low-pass bandgap of filer are filtered out and are not allowed to pass. Moreover, the added filter has no effect on the resonant wavelength position of the fundamental mode of the cavity sensor. Here, it should be noted that if the band edge modes of the bandgap filter (1-D PC-NBF) do not match the fundamental mode of the 1-D PC-NCS, the side lobe in transmission spectrum of 1-D PC-NBF will lead to the offset of fundamental mode peak, which will bring in error. Actually, this problem can be solved by enhancing the cavity Q-factor of 1-D PC-NCS or enlarging the band gap width of 1-D PC-NBF.

As seen the transmission spectrum in Fig. 6(a), a high Q-factor of $\sim 2.2 \times 10^3$ and near 100% transmission for FM is obtained from 3D-FDTD calculation. To calculate the refractive index (RI) sensitivity (S) of the reported 1-D PC nanobeam integrated sensor device, the transmission spectra of the fundamental mode used for sensing are calculated when the background RI (including air-holes and ambient media) changes from RI = 1.0 to RI = 1.3 $(\Delta n = 0.3)$. As seen in Fig. 6(b) and (c), the resonant wavelength red-shift is $\Delta\lambda = 37$ nm. Therefore, the calculated RI sensitivity is $S = \Delta\lambda/\Delta n = 123.3$ nm/RIU. This agrees very well with our previous analysis obtained from Section 3, which confirms that the additional series-connected 1-D PC filter has no influence on the properties of FM (e.g., its Q-factor, resonance position and RI sensitivity).

Herein, it is worth mentioning that the footprint of the proposed 1-D PC nanobeam integrated sensor is ultra-compact $\sim 0.7\ \mu$m $\times$ 10 μm, more than three orders of magnitude improved compared with the integrated sensor devices based on 2-D PC [28], [29]. Thus, the method proposed in this work is more attractive and promising in future optical high-density multiplexed gas sensing and nanophotonic integration. In addition, compared with 2-D PC cavity or other split-mode microcavity [34] integrated sensor devices, the structures of the proposed single 1-D PC nanobeam cavity sensor devices are much more simple and easier to fabricate, which makes it

easy to build lab-on-chip densely integrated sensors array for accurate sensing with high parallel-multiplexing capability.

5. Conclusion

In summary, we have reported a method for integration of 1-D PC nanobeam bandgap filter and 1-D PC nanobeam cavity sensor. With 3-D-FDTD simulations, we discussed the shutoff frequency sharpness of the filter low-pass band as a function of the air-hole gratings number (N). In addition, a 1-D PC-NBF with wide low-pass band ranging from 1533 nm~1785 nm (with width $>$ 250 nm) is obtained when $N = 15$. Then, by connecting an additional 1-D PC nanobeam filter to a 1-D PC nanobeam sensor in series, a transmission only containing the fundamental mode for sensing detection is created. Moreover, the additional filter has no influence on the properties of the fundamental mode (e.g., *Q*-factor, resonance position and sensitivity). In particular, the footprint of the proposed 1-D PC nanobeam integrated sensor is ultra-compact, i.e., $\sim 0.7\ \mu\text{m} \sim 10\ \mu\text{m}$, which is more than three orders of magnitude decreased compared with 2-D PC integrated sensor devices. Thus, we believe that the method presented here may enhance the high integration performance of ultra-compact integrated sensor-array devices and other photonic integrated devices based on 1-D PC nanobeam elements.

Acknowledgment

D. Yang thanks Dr. Q. Quan from Rowland Institute, Harvard University, Cambridge, MA, USA for useful discussions and helpful comments. Thanks also to A. Shneidman from the group of Prof. M. Lončar at Harvard University for improving the English of the paper.

References

[1] J. Robinson, C. Manolatou, L. Chen, and M. Lipson, "Ultrasmall mode volumes in dielectric optical microcavities," *Phys. Rev. Lett.*, vol. 95, no. 14, Sep. 2005, Art. no. 143901.
[2] P. Velha *et al.,* "Ultra-high Q/V Fabry-Perot microcavity on SOI substrate," *Opt. Exp.*, vol. 15, no. 24, pp. 16090–16096, Nov. 2007.
[3] J. D. Ryckman and S. M. Weiss, "Low mode volume slotted photonic crystal single nanobeam cavity," *Appl. Phys. Lett.*, vol. 101, no. 7, Aug. 2012, Art. no. 071104.
[4] E. Kuramochi *et al.,* "Ultrahigh-*Q* one-dimensional photonic crystal nanocavities with modulated mode-gap barriers on SiO_2 claddings and on air claddings," *Opt. Exp.*, vol. 18, no. 15, pp. 15859–15869, Jul. 2010.
[5] Q. Quan, P. B. Deotare, and M. Loncar, "Photonic crystal nanobeam cavity strongly coupled to the feeding waveguide," *Appl. Phys. Lett.*, vol. 96, no. 20, May 2010, Art. no. 203102.
[6] Y. Li, C. Wang, and M. Loncar, "Design of nano-groove photonic crystal cavities in lithium niobate," *Opt. Lett.*, vol. 40, no. 12, pp. 2902–2905, Jun. 2015.
[7] A. Bazin, R. Raj, and F. Raineri, "Design of silica encapsulated high-Q photonic crystal nanobeam cavity," *J. Lightw. Technol.*, vol. 32, no. 5, pp. 952–958, Mar. 2014.
[8] P. Lee, T. Lu, and L. Chiu, "Dielectric-band photonic crystal nanobeam lasers," *J. Lightw. Technol.*, vol. 31, no. 1, pp. 36–42, Jan. 2013.
[9] X. Ge, Y. Shi, and S. He, "Ultra-compact channel drop filter based on photonic crystal nanobeam cavities utilizing a resonant tunneling effect," *Opt. Lett.*, vol. 39, no. 24, pp. 6973–6976, Dec. 2014.
[10] J. Hendrickson, R. Soref, J. Sweet, and W. Buchwald, "Ultrasensitive silicon photonic-crystal nanobeam electro-optical modulator: Design and simulation," *Opt. Exp.*, vol. 22, no. 3, pp. 3271–3283, Feb. 2014.
[11] S. Lin, J. Hu, L. Kimerling, and K. Crozier, "Design of nanoslotted photonic crystal waveguide cavities for single nanoparticle trapping and detection," *Opt. Lett.*, vol. 34, no. 21, pp. 3451–3453, Nov. 2009.
[12] T. Lin, C. Lin, and J. Hsu, "Strong optomechanical interaction in hybrid plasmonic-photonic crystal nanocavities with surface acoustic waves," *Sci. Rep.*, vol. 5, Sep. 2015, Art. no. 13782.
[13] Y. Zhang *et al.,* "Single-mode emission from Ge quantum dots in photonic crystal nanobeam cavity," *IEEE Photon. Technol. Lett.*, vol. 27, no. 9, pp. 1026–1029, May 2015.
[14] R. Miura *et al.,* "Ultralow mode-volume photonic crystal nanobeam cavities for high-efficiency coupling to individual carbon nanotube emitters," *Nat. Commun.*, vol. 5, Nov. 2014, Art. no. 5580.
[15] Y. Li *et al.,* "Photonic crystal nanobeam cavity with stagger holes for ultrafast directly modulated nano-light-emitting diodes," *IEEE Photon. J.*, vol. 5, no. 1, Feb. 2011, Art. no. 4700306.
[16] S. Makino, Y. Ishizaka, K. Saitoh, and M. Koshiba, "Slow-light-enhanced nonlinear characteristics in slot waveguides composed of photonic crystal nanobeam cavities," *IEEE Photon. J.*, vol. 5, no. 2, Apr. 2013, Art. no. 2700309.
[17] R. Daw and J. Finkelstein, "Lab on a chip," *Nature*, vol. 442, no. 7101, pp. 367–418, 2006.

[18] D. Yang, P. Zhang, H. Tian, Y. Ji, and Q. Quan, "Ultrahigh-*Q* and low mode volume parabolic radius-modulated single photonic crystal slot nanobeam cavity for high-sensitive refractive index sensing," *IEEE Photon. J.*, vol. 7, no. 5, Oct. 2015, Art. no. 4501408.
[19] S. Kim, H. Kim, and Y. Lee, "Single nanobeam optical sensor with a high *Q*-factor and high sensitivity," *Opt. Lett.*, vol. 40, no. 22, pp. 5351–5354, Nov. 2015.
[20] D. Yang, H. Tian, and Y. Ji, "High-*Q* and high-sensitivity width-modulated photonic crystal single nanobeam air-mode cavity for refractive index sensing," *Appl. Opt.*, vol. 54, no. 1, pp. 1–5, Jan. 2015.
[21] D. Yang, H. Tian, Y. Ji, and Q. Quan, "Design of simultaneous high-*Q* and high-sensitivity photonic crystal refractive index sensors," *J. Opt. Soc. Amer. B, Opt. Phys.*, vol. 30, no. 8, pp. 2027–2031, Aug. 2013.
[22] C. Wang, Q. Quan, S. Kita, Y. Li, and M. Lončar, "Single-nanoparticle detection with slot-mode photonic crystal cavities," *Appl. Phys. Lett.*, vol. 106, no. 26, Jun. 2015, Art. no. 261105.
[23] Q. Quan *et al.,* "Single particle detection in CMOS compatible photonic crystal nanobeam cavities," *Opt. Exp.*, vol. 21, no. 26, pp. 32225–32233, Dec. 2013.
[24] D. Yang *et al.,* "High sensitivity and high *Q*-factor nanoslotted parallel quadrabeam photonic crystal cavity for real-time and label-free sensing," *Appl. Phys. Lett.*, vol. 105, no. 6, Aug. 2014, Art. no. 063118.
[25] F. Liang, N. Clarke, P. Patel, M. Loncar, and Q. Quan, "Scalable photonic crystal chips for high sensitivity protein detection," *Opt. Exp.*, vol. 21, no. 26, pp. 32306–32312, Dec. 2013.
[26] L. J. Sherry, S. Chang, G. C. Schatz, and R. P. Van Duyne, "Localized surface plasmon resonance spectroscopy of single silver nanocubes," *Nano Lett.*, vol. 5, no. 10, pp. 2034–2038, Oct. 2005.
[27] Q. Quan and M. Loncar, "Deterministic design of wavelength scale, ultra-high Q photonic crystal nanobeam cavities," *Opt. Exp.*, vol. 19, no. 19, pp. 18529–18542, Sep. 2011.
[28] D. Yang, H. Tian, and Y. Ji, "Nanoscale photonic crystal sensor arrays on monolithic substrates using side-coupled resonant cavity arrays," *Opt. Exp.*, vol. 19, no. 21, pp. 20023–20034, Oct. 2011.
[29] H. Yan *et al.,* "Silicon on-chip bandpass filters for the multiplexing of high sensitivity photonic crystal microcavity biosensors," *Appl. Phys. Lett.*, vol. 106, no. 12, Mar. 2015, Art. no. 121103.
[30] W. Bogaerts *et al.,* "Silicon-on-insulator spectral filters fabricated with CMOS technology," *IEEE J. Sel. Topics Quantum Electron.*, vol. 16, no. 1, pp. 33–44, Jan./Feb. 2010.
[31] F. Xia, M. Rooks, L. Sekaric, and Y. Vlasov, "Ultra-compact high order ring resonator filters using submicron silicon photonic wires for on-chip optical interconnects," *Opt. Exp.*, vol. 15, no. 19, pp. 11934–11941, Sep. 2007.
[32] X. Wang *et al.,* "Narrow-band waveguide Bragg gratings on SOI wafers with CMOS-compatible fabrication process," *Opt. Exp.*, vol. 20, no. 14, pp. 15547–15558, Jul. 2012.
[33] J. D. Joannopoulos, S. G. Johnson, J. N. Winn, and R. D. Meade, *Photonic Crystals: Molding the Flow of Light*. 2nd ed. Princeton, NJ, USA: Princeton Univ. Press, 2008.
[34] B. Li *et al.,* "Single nanoparticle detection using split-mode microcavity Raman lasers," *Proc. Nat. Acad. Sci. USA*, vol. 111, no. 41, pp. 14657–14662, Oct. 2014.